Interlayer jump diffusion in the smectic-C_A^* phase by angular-dependent ^{2}H NMR study

J. Xu,[1] C. A. Veracini,[2] and Ronald Y. Dong[1,3]
[1]*Department of Physics and Astronomy, University of Manitoba, Winnipeg, Manitoba, Canada R3T 2N2*
[2]*Departimento di Chemicae Chimica Industriale, Universita di Pisa, Via Risorgimento 35, 56126, Pisa, Italy*
[3]*Department of Physics and Astronomy, Brandon University, Brandon, Manitoba, Canada R7A 6A9*
(Received 26 July 2005; published 3 November 2005)

A detailed ^{2}H nuclear magnetic resonance (NMR) study at 61.4 MHz of two chiral smectic *C* phases of a smectogen 10B1M7, one ferroelectric (SmC^*) and the other antiferroelectric (SmC_A^*), is reported. Simulation of angular-dependent spectral patterns and/or signal intensities of the methyl deuterons are shown to provide information on the synclinic or anticlinic ordering, as well as the jump diffusion rates at different temperatures in the SmC_A^* phase. The molecular self-diffusion constant is determined to be in the range of 0.2–1.2 $\times 10^{-14}$ m^2/s over the temperature range of the SmC_A^* phase. Molecular self-diffusion in the SmC^* phase should be faster, but remains undetectable by the present approach. Furthermore, the phase biaxiality in these phases is found to be vanishingly small. The critical magnetic field for unwinding the helical structure of 10B1M7 is found to be relatively high.

DOI: 10.1103/PhysRevE.72.051703 PACS number(s): 61.30.−v

I. INTRODUCTION

Since the discovery of chiral smectic phases in chiral liquid crystals (LC) [1], significant experimental and theoretical efforts have been directed to investigate the structure and dynamics of these materials [2–6]. However, among these chiral phases, only the structure of ferroelectric smectic C^* (SmC^*) and antiferroelectric smectic C^* (SmC_A^*) were well understood. The helical structure of a SmC^* phase in some chiral materials may show solitonlike distortions when placed in a high magnetic field, that is, the structure now contains wide regions of nearly uniform twist separated by narrow solitonlike regions of twist. A herringbonelike structure is seen in SmC_A^* phase, i.e., the molecular tilt angle is the same but the tilt directions alternate by π in the two neighboring layers. For other chiral phases and subphases (e.g., SmC_α^*, SmC_{Fi}^*), the general feature of their structures is still not clear. Two popular structure models were proposed, "clock" model and "Ising-type" model [5,7,8]. Among them, the clock model is supported by most of the experiments. The SmC_α^* phase has a clocklike structure, in which the director rotates by a constant azimuthal angle in the consecutive layers. The ferrielectric SmC_{Fi}^* phase has a distorted clocklike structure with three- or four-layer periodicity [9]. It occurs between the synclinic SmC^* phase and anticlinic SmC_A^* phase. A recent work has indicated that the ferrielectric phase is nearly Ising-type [10]. Besides x-ray scattering techniques [6] and dynamic light scatterings [11], angular dependent ^{2}H NMR has been proven to be a powerful tool with which to study the molecular arrangements in the LC phases, and to even extract dynamical information [4,12,13]. Furthermore, we have recently used this technique to study solitonlike distortions in the SmC^* phase of a chiral smectogen 8BEF5 by the NMR magnetic field (H), and to produce a partial (H,T) phase diagram [14].

In the present paper, we use angular-dependent ^{2}H NMR to investigate the structure and dynamics in the SmC^* and SmC_A^* phases of 1-methylheptyl 4'-(4-n-decyloxybenzoyloxy)-biphenyl-4-carboxylate(10B1M7). It is our aim in this study to further demonstrate the power of deuterium angular-dependent spectral patterns and signal intensities, and to show its potential in addressing the structural models of other exotic tilted chiral phases. The paper is organized as follows. Section II gives the relevant theory to describe simulations of experimental results, and to extract interlayer jump diffusion constants in the SmC_A^* phase. Section III contains the experimental method, while Sec. IV gives the results and discussion. The last section gives a brief conclusion.

II. THEORY

It is well known that molecules are moving in a fast motion regime in liquid crystalline phases. In aligned deuterated liquid crystals (LC), the ^{2}H spin(s) can give rise to a spectrum of two lines with spectral frequencies given by [15]

$$\nu^{\pm} = \pm \frac{3}{4}\bar{\nu}_Q\left(\frac{3}{2}\cos^2\beta - \frac{1}{2} + \frac{\bar{\eta}}{2}\sin^2\beta\cos 2\alpha\right), \qquad (1)$$

where $\bar{\eta}$ is a time-averaged asymmetry parameter, $\bar{\nu}_Q = eQ\bar{V}_{zz}/h$ is a time-averaged nuclear quadrupolar coupling constant along the long molecule (Z_M) axis, and β, α are the polar angles of the applied magnetic field in the molecule frame (see Fig. 1). For the angular-dependent study of chiral *C* phases, β can be obtained from the geometry to give

$$\cos\beta = \sin\theta\sin\theta_0\cos\phi + \cos\theta\cos\theta_0, \qquad (2)$$

where θ is rotation angle, θ_0 is the molecular tilt angle, and ϕ is the molecular azimuthal angle measured with respect to the plane formed by the layer normal and the magnetic field (i.e., x axis in Fig. 1). In the SmC^* phase, the pitch axis is aligned along the external magnetic field. When the pitch axis is set at nonzero θ angle, the observed spectrum is the sum of frequencies from the molecules in the helical structure which are uniformly distributed on the surface of the

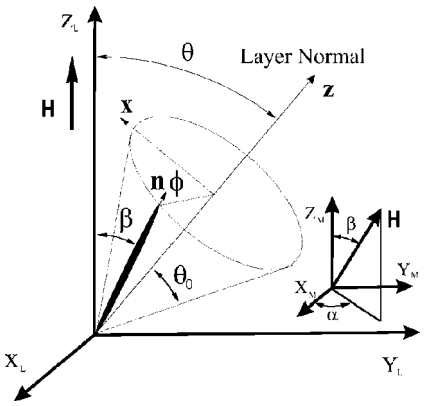

FIG. 1. The geometry of a sample rotation experiment. **n** is the molecular director. (X_L, Y_L, Z_L) is the laboratory frame, (X_M, Y_M, Z_M) is the molecular frame, whereas the (x,y,z) frame is fixed to the LC smectic layers.

cone shown in Fig. 1 [15], thereby producing two or three singularities (s_1, s_2, s_3). $\bar{\eta}$, $\bar{\nu_Q}$, and θ_0 can be determined by fitting the angular-dependent positions of the singularities using [15]

$$s_1^{\pm} = \pm\frac{3}{4}\bar{\nu}_Q\left[1-\frac{1}{2}(3-\bar{\eta})\sin^2(\theta-\theta_0)\right],$$

$$s_2^{\pm} = \pm\frac{3}{4}\bar{\nu}_Q\left[1-\frac{1}{2}(3-\bar{\eta})\sin^2(\theta+\theta_0)\right],$$

and when $\pi/2 \geqslant \theta \geqslant \tan^{-1}\{(3-\bar{\eta})\sin 2\theta_0/[(3-\bar{\eta})2\sin^2\theta_0 + 4\bar{\eta}]\}$

$$s_3^{\pm} = \pm\frac{3}{4}\bar{\nu}_Q\left[\frac{(3+\bar{\eta})\bar{\eta}\cos^2\theta}{(3-\bar{\eta})\sin^2\theta_0 + 2\bar{\eta}} - \frac{1}{2}(1+\bar{\eta})\right]. \quad (3)$$

Notice that $s_3^{\pm}$ is a corrected version of Ref. [15].

If a uniform ϕ distribution in the helix is distorted by the NMR magnetic field resulting in a ϕ distribution $[d\phi/dz \propto f_{DIST}(\phi)]$ [16], the critical field (H_c) for unwinding the helical structure in the SmC^* phase can be obtained by fitting the distorted spectra using the Fourier transform of the free induction decay (FID) calculated by using Eqs. (1)–(2) in the following integral [14,16]:

$$G(t) = G(0)\int_0^{2\pi}\frac{1}{f_{DIST}(\phi)}\cos[2\pi\nu(\phi,\theta,\theta_0)t]e^{-\sigma^2t^2/2-t/T_2^*}d\phi, \quad (4)$$

where $\exp(-\sigma^2t^2/2 - t/T_2^*)$ is to account for the spectral line broadening which is governed by fitting parameters σ, and T_2^*, $f_{DIST}(\phi) = \sqrt{1+1/(4A)-\kappa^2[\cos 2\phi/(4A)+\cos\phi]}$ with $A = \cot\theta\cot\theta_0$, $\kappa(H/H_c,\theta)$ is a fitting parameter which is related to the critical field H_c and rotation angle by [14]

$$\frac{e(\kappa)}{\kappa} = \sqrt{\frac{\tan\theta_0}{\sin 2\theta}}\frac{4H_C}{H}, \quad (5)$$

with $e(\kappa) = \int_0^{2\pi} f_{DIST}(\phi)d\phi$, and H_C is the critical field to unwind the helix when it is applied normal to the pitch axis.

In the SmC_A^* phase, the tilt direction of the molecules in the two neighboring layers is opposite and the interlayer jump caused by molecular self-diffusion will modulate the nuclear quadrupolar interaction(s). Such modulations, however, are unobservable by NMR in the SmC^* phase [4]. The ^{2}H spectra in SmC_A^* phase can be described by a two-sites jump problem where the resonant frequencies for the two sites are $2\pi\nu(\phi)$ and $2\pi\nu(\pi+\phi)$, respectively. The jump between two neighboring sites is taken as a stochastic process. Then, the free precession evolution of the magnetization can be described by the Bloch-McConnell equation [17,18]

$$\frac{d\mathbf{M}}{dt} = [\mathbf{\Lambda}+\mathbf{\Gamma}]\mathbf{M}, \quad (6)$$

where **M** is a column vector with components M_a and M_b for the two sites a and b. $\mathbf{\Lambda}$ is defined by the spin Hamiltonian of the system and $\mathbf{\Gamma}$ is a matrix describing the stochastic jump process between the two sites. In our case, the spin Hamiltonian is the quadrupolar interaction, and

$$\mathbf{\Lambda}+\mathbf{\Gamma} = \begin{pmatrix} -i2\pi\nu(\phi)-2\Omega & 2\Omega \\ 2\Omega & -i2\pi\nu(\phi+\pi)-2\Omega \end{pmatrix} \quad (7)$$

where Ω is the probability of the molecule jumping from one layer to one of the two neighboring layers per unit time. So, the total magnetization formed by a solid echo sequence is [19]

$$\mathbf{M}(t) = e^{(\mathbf{\Lambda}+\mathbf{\Gamma})(t+\tau)}(e^{(\mathbf{\Lambda}+\mathbf{\Gamma})\tau}\mathbf{M}_0)^*, \quad (8)$$

where τ is the time interval between the $\pi/2$ pulses in the solid echo experiment [20]. The two neighboring sites are equivalent. Hence, $M_a(0) = M_b(0) = 1/2$ is taken for convenience, giving the initial condition $\mathbf{M}_0 = [1/2, 1/2]^T$. The exponentials in Eq. (8) can become tractable by means of matrix diagonalization [21]. For quadrature detection, the absorption signal for different ϕ angles is $G(\phi,t) = \mathrm{Re}[\mathbf{1}\cdot\mathbf{M}(t)]$, and the observed signal in SmC_A^* phase is a linear superposition of contributions from all layers over one pitch length. Thus

$$G_{tot}(t) = \frac{G_{tot}(0)}{4K(\kappa)}\int_0^{2\pi}\frac{G(\phi,t)e^{-\sigma^2t^2/2-t/T_2^*}}{\sqrt{1-\kappa^2\cos^2\phi}}d\phi, \quad (9)$$

where $K(\kappa)$ is the complete elliptic integral of the first kind, $1/\sqrt{1-\kappa^2\cos^2\phi}$ is the distribution of the azimuthal angle in the presence of external magnetic field [4], and the exponential function has been defined in Eq. (4). The ^{2}H NMR line shapes are simulated by numerically calculating the Fourier transform of Eq. (9) so as to obtain the interlayer jump rate. Note that when $\kappa = 0$, the field-induced distortion of the helix vanishes, and κ also can be related to the critical field H_c and rotation angle θ by [22]

$$\frac{E(\kappa)}{\kappa} = \frac{1}{\sin\theta}\frac{H_c}{H}, \quad (10)$$

where $E(k)$ is the complete elliptic integral of the second kind. Let us define

$$x = \delta\pi/\Omega, \quad \nu_0 = [\nu(\phi) + \nu(\phi+\pi)]/2, \tag{11}$$

where $\delta = |[\nu(\phi) - \nu(\phi+\pi)]/2|$. In the fast jump rate limit, i.e., $x \to 0$ or $\delta \ll \Omega$, the observed angular-dependent singularites in the SmC_A^* phase are given by taking $d\nu_0(\phi)/d\phi = 0$

$$\nu_1(\theta) = \pm\frac{3}{8}\bar{\nu}_Q[3(\sin^2\theta\sin^2\theta_0 + \cos^2\theta\cos^2\theta_0) - 1],$$
$$\nu_2(\theta) = \pm\frac{3}{8}\bar{\nu}_Q[3\cos^2\theta\cos^2\theta_0 - 1], \tag{12}$$

where $\bar{\eta}$ has been neglected. Note that the fast jump rate limit is satisfied when the rotation angle θ is close to 0° or 90°, since according to Eqs. (1) and (2) $\delta \to 0$.

It is well known that the solid echo signal will decay according to motions during the solid echo time τ [21]. So, an alternative method to find the jump rate would be to determine the decay rate of the solid-echo intensity $I(\theta, 2\tau)$ at different rotation angles. The angular-dependent echo intensities can be obtained from Eq. (9) to give

$$I(\theta,2\tau) = G_{tot}(0) = \frac{I(0,2\tau)}{4K(\kappa)}\int_0^{2\pi}\frac{G(\phi,0)}{\sqrt{1-\kappa^2\cos^2\phi}}d\phi. \tag{13}$$

An analytical form of $G(\phi,0)$ can be derived from Eq. (8) [21]. For slow exchange $x > 1$

$$G(\phi,0) = \frac{e^{-4\Omega\tau}}{(x^2-1)}[-\cos(4\Omega\sqrt{x^2-1}\,\tau) + \sqrt{x^2-1}\,\sin(4\Omega\sqrt{x^2-1}\,\tau) + x^2], \tag{14}$$

while for fast exchange $x < 1$

$$G(\phi,0) = \frac{e^{-4\Omega\tau}}{(1-x^2)}[\cosh(4\Omega\sqrt{1-x^2}\,\tau) - \sqrt{x^2-1}\,\sinh(4\Omega\sqrt{1-x^2}\,\tau) - x^2]. \tag{15}$$

From Eqs. (14) and (15), it can be noticed that $I(\theta,2\tau)/I(0,2\tau)$ depends on κ, $\bar{\eta}$, $\Omega\tau$, $\bar{\nu}_Q/\Omega$, θ, and θ_0. In our solid-echo intensity study, κ and $\bar{\eta}$ are all set to 0. The numerically calculated echo amplitude as a function of θ is shown in Fig. 2 for two $\bar{\nu}_Q/\Omega$ values, where the parameters tilt angle $\theta_0 = 20°$ and jump rate $\Omega = 2$ kHz are set, and the echo amplitudes $I(\theta,2\tau)$ are normalized with respect to the echo intensity at $\theta = 0$, $I(0,2\tau)$. Equation (9) can be extended to the case of the Carr-Purcell pulse train, and the jump rate can also be extracted using the decay of the Carr-Purcell echoes.

III. EXPERIMENT

The chiral liquid crystal 10B1M7 shows various mesophases at different ranges of temperature. Its structure is sketched in Fig. 3(a), together with the deuteron labels. The synthesis and its characterization were reported elsewhere [23,24], and the transition temperatures of 10B1M7-d_{21}

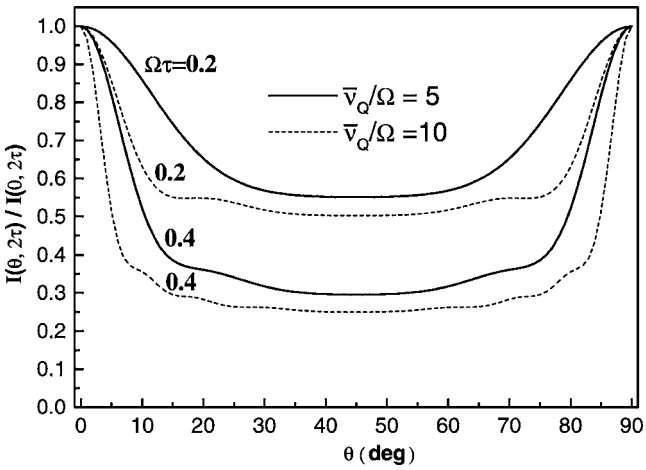

FIG. 2. The calculated echo amplitude as a function of θ for $\bar{\nu}_Q/\Omega = 5$ (solid lines) and $\bar{\nu}_Q/\Omega = 10$ (dotted lines) with $\Omega = 2$ kHz. The $\Omega\tau$ is a dimensionless variable with τ being the solid echo time. Two τ cases ($\Omega\tau = 0.2, 0.4$) are plotted as examples. The echo amplitudes $I(\theta,2\tau)$ are normalized with respect to the echo intensity at $\theta = 0$, $I(0,2\tau)$.

(deuterated on the achiral chain) determined by our ^{2}H NMR study were as follows:

$$\text{Iso} \overset{393K}{\leftrightarrow} \text{Sm}A \overset{373K}{\leftrightarrow} \text{Sm}C^* \overset{342.5K}{\leftrightarrow} \text{Sm}C_{Fi}^* \overset{330.3K}{\leftrightarrow} \text{Sm}C_A^* \overset{312.1K}{\leftrightarrow} \text{Sm}J^*.$$

The sample was aligned by cooling slowly to the desired temperature in the SmC^*/SmC_A^* phase after heating to the clearing temperature. Note that the intrigue SmC_{Fi}^* phase(s) deserves more attention and will not be the subject of the present investigation. The deuterium spectral patterns were

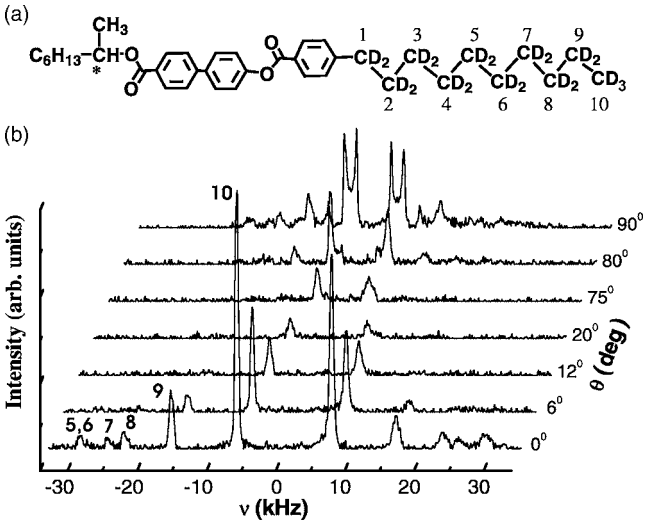

FIG. 3. (a) Molecular structure of a partially deuterated 10B1M7 with deuteron site labels. The asterisk indicates the chiral carbon center. (b) Typical ^{2}H NMR spectra collected at some θ values in the SmC_A^* phase of 10B1M7 at $T = 323.3$ K and $\tau = 800$ μs. Deuteron sites are assigned and labeled on the spectrum ($\theta = 0$), in which signals from C_1–C_4 deuterons are too weak to appear.

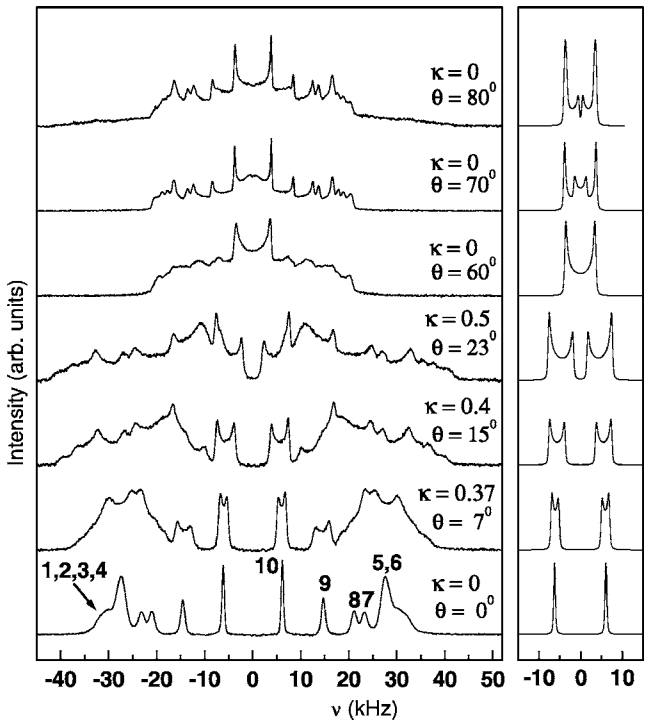

FIG. 4. Left: Typical experimental ^{2}H NMR spectra collected in the SmC^* phase of 10B1M7 at 345.8 K and τ=30 μs. Deuteron sites are assigned and labeled on the spectrum (θ=0). Right: Simulated line shapes for C_{10} deuterons using Eq. (4) with θ_0=21°, $\bar{\nu}_Q$=10.3 kHz, σ=1 kHz, and T_2^*=1.4 ms ($\bar{\eta}$, has been neglected). The κ values used in the simulation are listed in the left panel.

taken using a Bruker goinometer probe equipped with a high-precision pneumatic motor (better than 0.1° resolution) and a Bruker Avance 400 solid-state system. The temperature of the sample was regulated with an airflow to within 0.1 deg accuracy. A $90^\circ_x-\tau-90^\circ_y-\tau$ solid echo pulse sequence was used to generate ^{2}H spectra, and to give the echo maximum intensities at different rotation angles. The 90° pulse width was 3 μs. Typical number of scans needed to observe the FID or its Fourier transform was 128, and the recycle time between scans was 1.5 s. In the SmC_A^* phase, our experiments show that there are no observable field-induced sample reorientation and layer destruction in the studied θ region of 0°–90°. However, in the SmC^* phase, the sample did show obvious field-induced reorientation at high rotation angles (>60°). This is because the anticlinic order is far less sensitive to the external magnetic field than synclinic ordering [4]. The spectra in the SmC^* phase were collected only at its low-temperature end. Also, the spectra were collected immediately (<1 s) after rotating to a high θ angle in order to avoid any possible time-dependent sample degradation because of orientational flow. Before collecting another spectrum at this or other rotation angle, the sample was first aligned by heating into the isotropic phase.

Figure 3(b) shows some typical spectra at different θ values in the SmC_A^* phase (T=323.3 K and τ=800 μs). Note that in the present study, we focus on the methyl deuterons at the last carbon site C_{10} whose spin-lattice relaxation times are the largest [25]. At the same time, it has been shown in

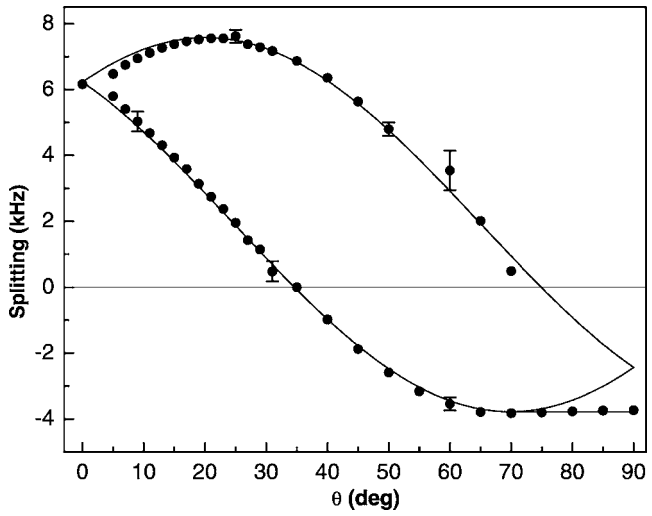

FIG. 5. Plot of the angular-dependent positions for the characteristic singularities of 10B1M7 at 345.8K(•). The solid lines are fitted curves using Eq. (3) to give $\bar{\nu}_Q$=10.1 kHz, θ_0=20.2°, and $\bar{\eta}$=0.

Fig. 2 that the echo intensity will decay faster when $\bar{\nu}_Q/\Omega$ is larger. Consequently, the measured echo intensities are essentially governed by the methyl group in the θ angle range of 6°–80°, and Eq. (13) can be safely used despite the fact that the achiral chain is fully deuterated (see Fig. 3).

IV. RESULTS AND DISCUSSION

A. Smectic-C^* phase study

The angular-dependent ^{2}H spectra collected in the SmC^* phase at 345.8 K and τ=30 μs are shown in Fig. 4, together with the simulated spectra for C_{10} deuterons using Eq. (4). The intensities of the experimental spectra were rescaled for clarity. The two characteristic singularities for SmC^* phase can be seen at nonzero rotation angles. The assignments of deuteron sites are also labeled on the spectrum(θ=0°). In simulating the spectra, θ_0=21°, $\bar{\nu}_Q$=10.3 kHz, σ=1 kHz, and T_2^*=1.4 ms were used for all rotation angles. The solitonlike distortion caused by the NMR magnetic field is hardly observed in the ^{2}H spectra (Fig. 4) [14], especially at high θ angles. This indicates that the critical field(H_c) for this sample is much higher than 9.4 T, even though nonzero κ values are used in some θ angles. However, deuteron peaks became overlapped when rotation angles were larger than 15°, thereby making a precise determination of the critical field (or κ) from the angular-dependent ^{2}H spectra almost impossible in our sample. A rough estimation of H_c=41±10 T is, however, obtained from κ=0.4(θ=15°) using Eq. (5). This value is about two times bigger than the H_c value for 8BEF5 [14]. $\bar{\eta}$ is also a small number and is therefore set to 0 in our fittings. The angular-dependent positions of the characteristic singularities are shown in Fig. 5 for the same temperature. The solid lines are fitted curves using Eq. (3) to give $\bar{\nu}_Q$=10.1 kHz, θ_0=20.2°, and $\bar{\eta}$=0. The fitting is excellent except in the small angle region (<10°) and perhaps in the large angle region. At the low angles, line broad-

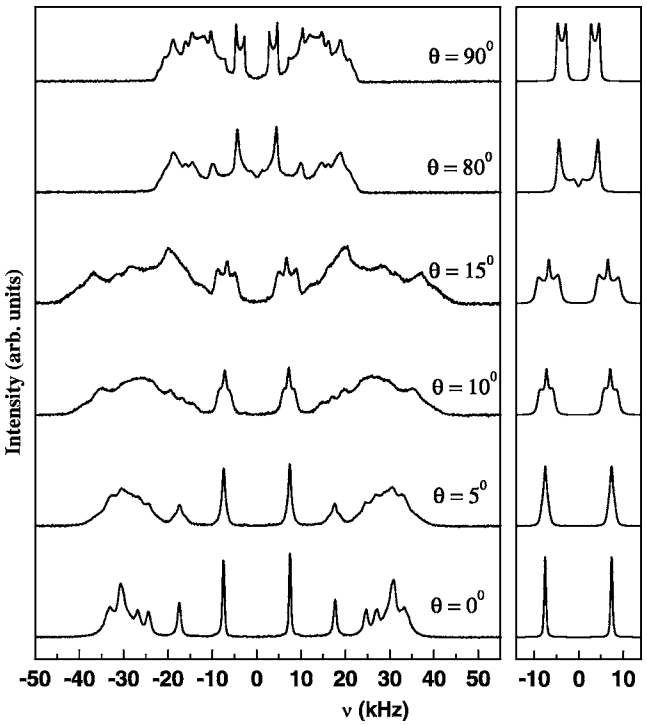

FIG. 6. Left: Experimental ^{2}H NMR spectra collected in the SmC_A^* phase of 10B1M7 at 323.3 K and τ=30 μs. Right: Simulated line shapes for C_{10} deuterons using Eq. (9) with the parameters given in Table I (κ=0 for all the simulations).

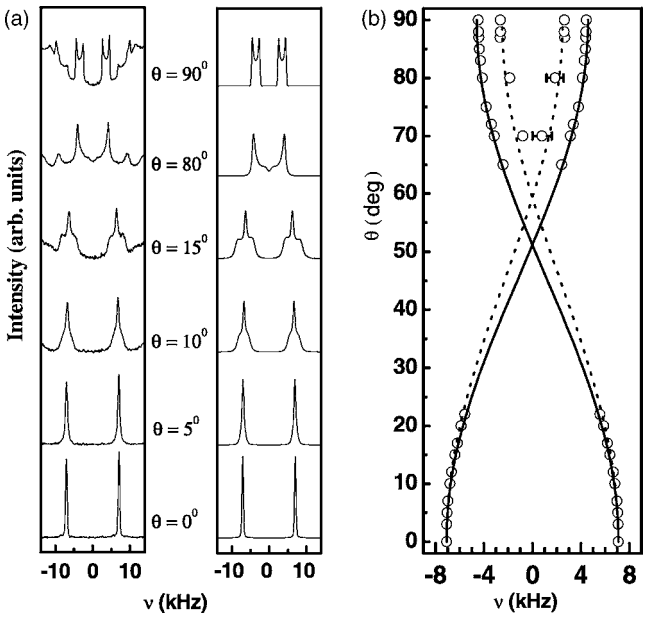

FIG. 7. (a) Left: Typical experimental ^{2}H NMR spectra (expanded region shown) collected in the SmC_A^* phase of 10B1M7 at 328 K and τ=30 μs. Right: Simulated line shapes for C_{10} deuterons using Eq. (9) with the parameters given in Table I, κ=0 were used. (b) Plot of experimental singularities(°) versus the θ angle at 328 K. Solid and dashed lines are theoretical curves according to ν_1, ν_2 [Eq. (12)], respectively, using the θ_0 and $\bar{\nu}_Q$ values given in Table I.

ening and the small separation between two singularities cause a somewhat larger experimental uncertainty. At the large angle region, overlap from signals due to other deuterated sites could cause some experimental errors. Indeed, fitting the singularities gives more accurate $\bar{\nu}_Q$ and θ_0 than the line shape fitting, but their values obtained by the two methods are consistent within the experiment error. We note that $\bar{\eta}$ is too small in 10B1M7 to be detected using the angular-dependent ^{2}H NMR study. Therefore, $\bar{\eta}$ is neglected in the following SmC_A^* phase study.

B. Smectic-C_A^* phase study

In the SmC_A^* phase, the angular-dependent ^{2}H spectra were collected with τ=30 μs at temperatures between 323 and 331 K. Figure 6 and Fig. 7(a) show the spectra collected at 323.3 and 328 K, respectively. Typical simulated C_{10} deuterons spectra using Eq. (9) are plotted in the right panel of these figures. The intensities of the experimental spectra were rescaled for clarity. In the small rotation angle region, these spectra show a doublet each with a central peak plus two shoulders. The shoulders come from the ϕ angle distribution of the molecules, which is the same as in the SmC^* phase, and the central peak results from motional narrowing due to interlayer jumps of the molecules. Comparing the spectra at different temperatures, one can notice that the intensities of the central peaks are stronger and the shoulders' intensities are lower when the jump rate is higher. Therefore, by fitting the line shapes, the jump rate can be obtained. The parameters used for the fittings are listed in Table I. Figure 7(b) shows the plot of experimental singularities(◦) versus the θ angle at 328 K, while solid and dashed lines are theoretical curves according to Eq. (12) using the values of θ_0 and $\bar{\nu}_Q$ given in Table I. It demonstrates that the parameters obtained by line shape fitting are indeed very reliable. As stated in Sec. IV A, the solitonlike distortion in SmC^* phase is almost unobservable. κ=0 was used for all the simulations. The interlayer self-diffusion constant can be related to jump rate by $D_{||}^{free}=4L^2\Omega/\pi^2$ (L is the layer thickness) under the assumption that the molecule can freely diffuse to the two neighboring layers (see the Appendix). If the interlayer diffusion is not free, the system can be treated by considering the molecules diffusing through an array of stacked planar membranes [26]. Then, the measured interlayer diffusion $D_{||}$ will be less than $D_{||}^{free}$. Since the layer

TABLE I. Parameters used for simulating line shapes.

Temp. (K)	σ (kHz)	T_2^* (ms)	θ_0 (deg)	$\bar{\nu}_Q$ (kHz)	Ω (kHz)
328	0.4±0.2	1±0.3	23±0.5	12.3±0.2	1.8±0.3
323.3	1±0.2	1.2±0.3	22.8±0.5	12.9±0.2	1.1±0.2

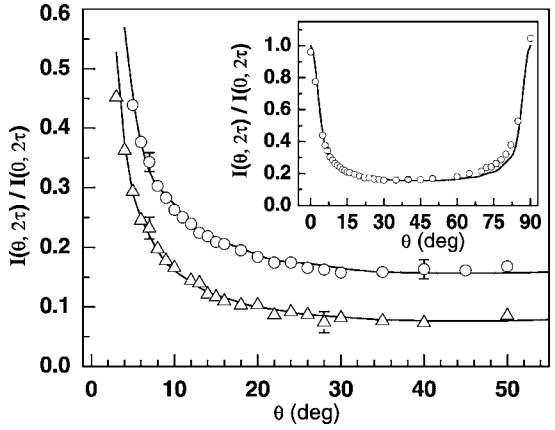

FIG. 8. Experimental normalized echo intensities $I(\theta,2\tau)/I(0,2\tau)$ versus the rotation angle θ for $\tau=400$ μs ($\circ$) and $\tau=600$ μs ($\triangle$) at 328 K. The fitting curves are calculated according to Eq. (13) with Ω and $I(0,2\tau)$ being the fitting parameters ($\kappa=0, \bar{\eta}=0$). The θ_0 and $\bar{\nu}_Q$ values given in Table I were used. In the inset, the normalized echo intensities($\circ$) and calculated curve are plotted for θ between 0° to 90° and $\tau=400$ μs.

thickness L is unknown for 10B1M7, $L=3.4$ nm is chosen from a similar LC [7] to estimate the $D_{\|}^{free}$ value. It is found that $D_{\|}^{free}(328\ \mathrm{K})=0.85\pm0.15\times10^{-14}$ m^2/s and $D_{\|}^{free}(323.3\ \mathrm{K})=0.5(2)\pm0.1\times10^{-14}$ m^2/s. These values are much smaller than the values found in other SmC_A^* phases [4]. However, they have the same order of magnitude as the values found in columnar liquid crystalline phase, i.e., $1.2-3.8\times10^{-14}$ m^2/s [27]. To demonstrate the method of extracting jump rate from the solid echo decay ratio, Figs. 8 and 9 show $I(\theta,2\tau)/I(0,2\tau)$ versus the rotation angle (between 0° and 55°) for two different temperatures. The solid curves shown in these figures are calculated according to Eq. (13) with Ω and $I(0,2\tau)$ being the fitting parameters ($\kappa=0, \bar{\eta}=0$), while the θ_0 and $\bar{\nu}_Q$ values given in Table I were used. The inset in Fig. 8 shows the echo intensities measured for θ from 0° to 90° with $\tau=400$ μs and

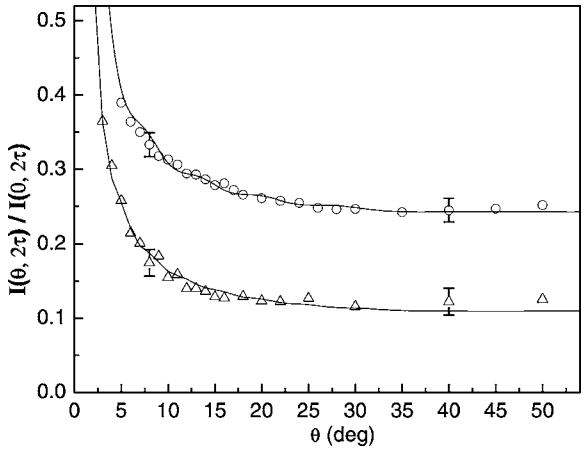

FIG. 9. Experimental normalized echo intensities $I(\theta,2\tau)/I(0,2\tau)$ versus the rotation angle θ for $\tau=500$ μs ($\circ$) and $\tau=800$ μs ($\triangle$) at 323.3 K. The fitting curves are calculated as in Fig. 8.

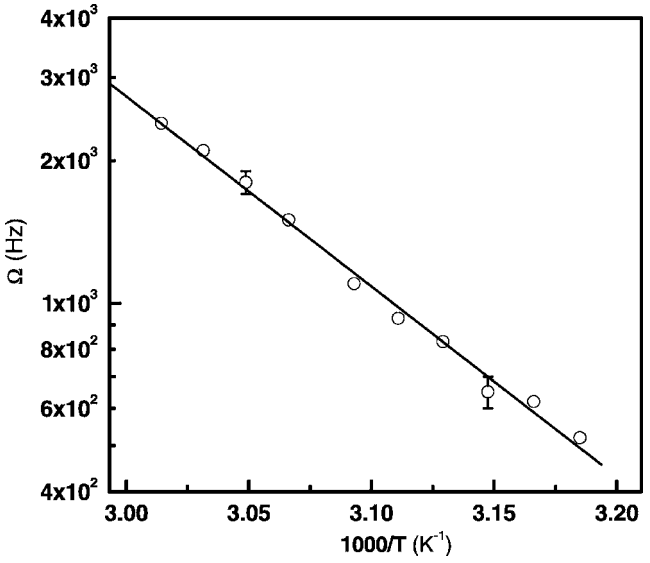

FIG. 10. Arrhenius plot of the jump rate Ω ($\circ$) measured by line shape fitting for the temperatures between 314 and 330 K. The solid line is a linear fitting curve for the Ω.

328 K. The intensities in the high rotation angle region ($55°<\theta<85°$) are slightly higher than predicted by the fitted curve. This may be caused by the orientational flow of molecules in the NMR magnetic field. Therefore, in these figures our fittings were limited to a smaller rotation angle region, usualy less than 55°. Since our sample is perdeuterated in the achiral chain, this echo intensity method is only feasible for large τ values ($\tau\geqslant400$ μs). Otherwise, the solid echo intensities will be complicated by those sites containing methylene deuterons (see Sec. II). $\Omega(328\ \mathrm{K})=1.5$ kHz and $\Omega(323.3\ \mathrm{K})=0.8$ kHz were obtained from these intensity fittings. These jump rates Ω confirm the reliability of the line shape fitting method. Hence, in Fig. 10 the Ω values obtained solely by the line shape simulations are plotted as a function of the reciprocal temperature. It is seen that the self-diffusion or jump rate is a thermally activated process except for the pretransitional behavior near the transition to the ferrielectric phase. The solid line is the linear fitting curve for Ω at temperatures less than 332 K, and the slope gives the activation energy for the interlayer self-diffusion, i.e., about 77 kJ/mol. This value appears physically reasonable for the SmC_A^* phase. Translational self-diffusion has been reported [28] in 10B1M7 using a static fringe field of a superconducting magnet, giving $D_{\|}\approx0.5\times10^{-14}$ m^2/s in the SmC_A^* phase. This value is indeed consistent with those given above. It would be useful to apply modern pulse field gradient techniques [27] to measure the self-diffusion constant in 10B1M7 as a function of temperature for direct comparison with the results in Fig. 10.

V. CONCLUSION

The present study has demonstrated clearly the powerful technique of simulating angular dependent spectra of bulk LC to provide structural and dynamic information in the chiral C phases. In the SmC_A^* phase, the interlayer jump diffu-

sion can be studied by rotating the sample in the external magnetic field to give angular-dependent echo intensity and/or spectral pattern. The methods used here rely on chiral smectogens with suitable deuteration. As seen in the present study, it will be more advantageous to use a specifically deuterated carbon site on the chain (either C_{10} or C_1). A deuterated site on the chiral chain is also feasible for this study. The echo intensity study is less time consuming to obtain the jump constant, but in the present study we were limited to using quite a large τ value, which unfortunately causes lower echo maximum. We found that the phase biaxiality measured by $\bar{\eta}$ in the two chiral phases studied is too small to be detected. This is different from the case of SmC phase. It is noted that angular-dependent deuterium spectra can tell the local structure of the LC phase, e.g., SmC^* versus SmC_A^*. The potential of using the present NMR approach to discriminate various "clocklike" chiral phases is real. An account of the ferrielectric phase(s) of 10B1M7 using the methodology developed here will be detailed elsewhere.

ACKNOWLEDGMENTS

The Natural Sciences and Engineering Council of Canada, Canada Foundation of Innovation, and Brandon University are thanked for their financial support. C.A.V. acknowledges the support of Italian MIUR.

APPENDIX: RELATION BETWEEN INTERLAYER SELF-DIFFUSION CONSTANT $D_\parallel$ AND INTERLAYER JUMP RATE Ω

To consider interlayer diffusion, the smectic C_A^* phase can be treated as a number of alternating A (tilt direction ϕ) and B (tilt direction $\phi+\pi$) layers joined together to form a laminated structure, without considering the helical structure [4]. They have equal layer thickness L. First, "labeled" molecules are put in the A layers, and the time-dependent total labeled molecules in the region A can be derived from $dN(t)/dt=-2\Omega\{N(t)-[N_0-N(t)]\}$, where Ω is the probability per unit time for the labeled molecules to diffusion from one of A's layers to one of its neighboring B layers. Then, the time-dependent total number of labeled molecules in A is

$$N(t)=\frac{N_0}{2}e^{-4\Omega t}+\frac{N_0}{2}. \tag{A1}$$

Note that uniform distribution of the molecules in A and B layers was assumed in this derivation.

Second, the time-dependent distribution of molecules for this problem is obtained by solving Fick's second law of diffusion

$$\frac{dC(z,t)}{dt}=D_\parallel\frac{d^2C(z,t)}{dz^2}, \tag{A2}$$

where $C(z,t)$ is the molecule concentration. Obviously, for our case the molecular distribution is a periodic function, and the origin is put in the middle of one of the layers. The initial condition can be written as

$$C(z,t)=s_0(z)\quad\left(t=0,\quad nL-\frac{L}{2}<z<nL+\frac{L}{2}\right), \tag{A3}$$

where $s_0(z)$ is the steady-state molecular distribution in the A layers. Under the condition that the molecules can diffuse freely between these smectic layers, the time-dependent molecular distribution can be obtained from Eq. (A2) using Fourier series expansion [29]

$$C(z,t)=\frac{B_0}{2}+\sum_{n=1}^{\infty}B_n\cos\left(\frac{n\pi z}{L}\right)e^{[-(n^2\pi^2D)/L^2]t}, \tag{A4}$$

where B_n is given by $1/L\int_{-L/2}^{L/2}s_0(z)\cos[n(\pi z/L)]dz$. Hence, the total number of molecules in one layer is

$$N(t)=\int_{-L/2}^{L/2}C(z,t)dz=\frac{N_0}{2}+\sum_{n=1}^{\infty}\frac{2LB_n}{n\pi}\sin\left(\frac{n\pi}{2}\right)e^{[-(n^2\pi^2D_\parallel)/L^2]t}. \tag{A5}$$

The higher order terms usually decay rapidly. When $D_\parallel t/L^2>1$, the above equation can be simplified to [30]

$$N(t)\approx\frac{N_0}{2}+\frac{2LB_1}{\pi}e^{-(\pi^2D_\parallel/L^2)t} \tag{A6}$$

Comparing this with Eq. (A1) [30], self-diffusion constant $D_\parallel$ can now be related to jump rate Ω by

$$D_\parallel=\frac{4\Omega L^2}{\pi^2}. \tag{A7}$$

[1] R. B. Meyer, L. Liebert, L. Strzelecki, and P. Keller, J. Phys. (Paris) **36**, L69 (1975).
[2] V. L. Lorman, A. A. Bulbitch, and P. Toledano, Phys. Rev. E **49**, 1367 (1994).
[3] Y. Galerne and L. Liebert, Phys. Rev. Lett. **66**, 2891 (1991).
[4] B. Zalar, A. Gregorovic, and R. Blinc, Phys. Rev. E **62**, R37 (2000).
[5] P. V. Dolganov, V. M. Zhilin, V. K. Dolganov, and E. I. Kats, Phys. Rev. E **67**, 041716 (2003).
[6] P. Mach, R. Pindak, A.-M. Levelut, P. Barois, H. T. Nguyen, C. C. Huang, and L. Furenlid, Phys. Rev. Lett. **81**, 1015 (1998).
[7] A. Fukuda, Y. Takanishi, T. Isozaki, K. Ishikawa, and H. Takezoe, J. Mater. Chem. **4**, 997 (1994).
[8] P. M. Johnson, D. A. Olson, S. Pankratz, T. Nguyen, J. Goodby, M. Hird, and C. C. Huang, Phys. Rev. Lett. **84**, 4870 (2000).
[9] I. Musevic, B. Zeks, R. Blinc, T. Rasing, and P. Wyder, Phys. Rev. Lett. **48**, 192 (1982).
[10] E. Dzik, J. Mieczkowski, E. Gorecka, and D. Pociecha, J. Mater. Chem. **15**, 1255 (2005).
[11] D. Konovalov, H. T. Nguyen, M. Copic, and S. Sprunt, Phys. Rev. E **64**, 010704 (2001).

[12] N. A. Vaz, M. J. Vaz, and J. W. Doane, Phys. Rev. A **30**, 1008 (1984).
[13] J. Figueirinhas, S. Žumer, and J. W. Doane, Phys. Rev. A **35**, 4389 (1987).
[14] J. Xu, C. A. Veracini, and R. Y. Dong, Chem. Phys. Lett. (to be published).
[15] B. G. Wu and J. W. Doane, J. Magn. Reson. (1969-1992) **75**, 39 (1987).
[16] B. Zalar, A. Gregorovic, M. Simsic, A. Zidansek, R. Blinc, S. Keast, and M. Neubert, Phys. Rev. Lett. **80**, 4458 (1998).
[17] H. M. McConnell, J. Chem. Phys. **28**, 430 (1958).
[18] A. Abraham, *Principles of Nuclear Magnetism* (Oxford University Press, Oxford, 1986).
[19] A. J. Vega and Z. Luz, J. Chem. Phys. **42**, 1615 (1965).
[20] J. H. Davis, K. R. Jeffrey, M. Bloom, M. I. Valic, and T. P. Higgs, Chem. Phys. Lett. **42**, 390 (1976).
[21] K. Müller, R. Poupko, and Z. Luz, J. Magn. Reson. (1969-1992) **89**, 5877 (1990).
[22] P. J. Collings and M. Hird, *Introduction to Liquid Crystals* (Taylor & Francis, London, 1997).
[23] J. Goodby, J. Patel, and E. Chin, J. Mater. Chem. **2**, 197 (1992).
[24] D. Catalano, M. Cavazza, L. Chiezzi, M. Geppi, and C. Veracini, Liq. Cryst. **27**, 621 (2000).
[25] R. Y. Dong, L. Chiezzi, and C. A. Veracini, Phys. Rev. E **65**, 041716 (2002).
[26] J. E. Tanner, J. Chem. Phys. **69**, 1748 (1978).
[27] S. V. Dvinskikh, I. Furó, H. Zimmermann, and A. Maliniak, Phys. Rev. E **65**, 050702(R) (2002).
[28] M. Cifelli, V. Domenici, and C. A. Veracini, Mol. Cryst. Liq. Cryst. **429**, 167 (2005).
[29] J. Crank, *Mathematics of Diffusion* (Oxford University Press, Oxford, 1975).
[30] J. V. Sehy, A. A. Banks, J. J. H. Ackerman, and J. J. Neil, Biophys. J. **83**, 2856 (2002).